Anomalously Hot Electrons due to Rescatter of Stimulated Raman Scattering in the Kinetic Regime

B. J. Winjum, J. E. Fahlen, F. S. Tsung, and W. B. Mori

Phys. Rev. Lett. **110**, 165001 — Published 15 April 2013

DOI: 10.1103/PhysRevLett.110.165001

Anomalously Hot Electrons due to Rescatter of Stimulated Raman Scattering in the Kinetic Regime

B. J. Winjum,[1] J. E. Fahlen,[2] F. S. Tsung,[3] and W. B. Mori[1,3]

[1] *Department of Electrical Engineering, University of California Los Angeles, Los Angeles, CA 90095*
[2] *Areté Associates, Northridge, CA 91324*
[3] *Department of Physics and Astronomy, University of California Los Angeles, Los Angeles, CA 90095*

Using particle-in-cell simulations, we examine hot electron generation from electron plasma waves excited by stimulated Raman scattering and rescattering in the kinetic regime where the wavenumber times the Debye length ($k\lambda_D$) is $\gtrsim 0.3$ for backscatter. We find that for laser and plasma conditions of possible relevance to experiments at the National Ignition Facility (NIF), anomalously energetic electrons can be produced through the interaction of a discrete spectrum of plasma waves generated from SRS (back and forward scatter), rescatter, and the Langmuir decay of the rescatter-generated plasma waves. Electrons are bootstrapped in energy as they propagate into plasma waves with progressively higher phase velocities.

PACS numbers: 52.38.Bv, 52.35.Mw, 52.35.Fp, 52.65.-y

Stimulated Raman scattering (SRS), the decay of a light wave into a forward propagating electron plasma wave (EPW) and a forward (SRFS) or backward (SRBS) propagating light wave, involves fundamental nonlinear wave-wave and wave-particle interactions. SRS continues to be studied extensively because the loss of incoming energy due to backscatter and the potential fuel preheat due to hot electrons generated by the EPW are threats to Inertial Fusion Energy (IFE) devices such as the National Ignition Facility (NIF). Recent NIF experiments have shown electron heating up to energies above 100 keV [1]. A low-temperature (T_e = 10 - 20 keV) part of the heated electron distribution can be attributed to SRBS, but the high-temperature part is currently unexplained. There is speculation that these electrons are generated near the quarter-critical density by instabilities such as two-plasmon decay or SRFS [2].

In this article, we present a novel mechanism for generating 100 keV electrons through SRS rescatter, specifically through SRBS of SRBS, SRBS of SRFS, and the Langmuir decay instability (LDI) of rescatter EPWs, where LDI is the decay of an EPW into a counter-propagating EPW and an ion acoustic wave. We further show that electrons can get progressively heated as they travel between waves of increasing phase velocities. This mechanism allows rescatter and SRFS to heat electrons initially heated by SRBS, even though the SRFS EPW phase velocity is too high to trap and heat electrons on its own.

Particle-in-cell (PIC) simulations have been used to study rescatter and multi-stage electron heating from SRS, albeit multi-stage heating between SRBS and SRFS. Hinkel *et al.* [3] showed rescattering for NIF-relevant parameters but not the resulting hot electrons. Other authors [4–7] have shown electron heating by SRFS, in some cases explicitly due to SRFS accelerating electrons initially heated by SRBS, but these simulations were for more intensely-driven and/or hotter plasmas outside the current range for NIF where electron temperatures $T_e \approx$ 2-6 keV and laser intensities I and wavelengths λ_0 are such that $I\lambda_0^2 \approx 10^{14}$ W μm^2/cm^2 (in laser hot spots).

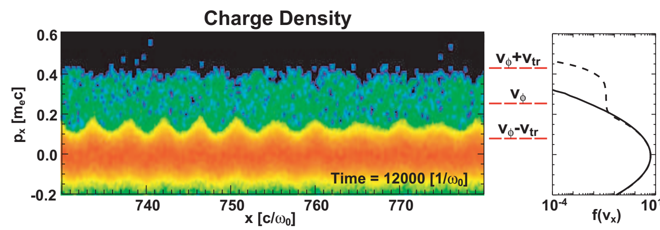

FIG. 1: Electron phasespace showing trapped particles during SRBS (left) with the corresponding flattening of the distribution function (right, dashed) and initial distribution (right, solid).

Electron energies that result from trapped particle interactions depend on the EPW's phase velocity, v_ϕ, and potential amplitude, Φ, with the trapped electron with the highest energy being that which oscillates between the top and bottom of the wave's potential well with potential difference $\Delta\Phi$. The maximum velocity v_{max} and energy $\mathcal{E}_{max}$ of a trapped electron can be obtained by considering that an electron's energy $\mathcal{E}$ is conserved in the wave ($'$) frame, with $\mathcal{E}' = (\gamma_v' - 1)mc^2 - e\Phi'$ where $\Phi' = \gamma_{v_\phi}\Phi$, $\gamma_v \equiv (1-(v/c)^2)^{-1/2}$, and e and m are the electron charge and mass respectively. In the non-relativistic limit, v_{max} is found to be $v_\phi + \sqrt{2e(\Delta\Phi)/m}$ and $\mathcal{E}_{max} = \frac{1}{2}mv_{max}^2$. For a sinusoidal EPW, $\Delta\Phi = 2\Phi_{max}$ and $v_{max} = v_\phi + v_{tr}$, with the trapping width $v_{tr} = 2\sqrt{e\Phi_{max}/m}$. Figure 1 illustrates trapped electrons oscillating between $v_{max} = v_\phi \pm v_{tr}$ in a kinetic SRS simulation (the first simulation below).

To estimate $\mathcal{E}_{max}$ as a function of $k\lambda_D$, the EPW wavenumber time the Debye length, we assume the EPW amplitude is bounded by the warm wavebreaking limit

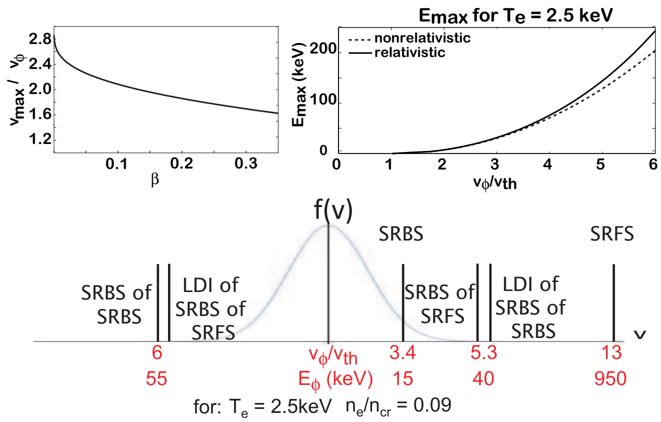

FIG. 2: Estimate of bound on maximum electron velocity v_{max} (top-left) and kinetic energy E_{max} (assuming $T_e = 2.5$ keV, top-right). EPW phase velocities for one set of parameters (bottom) illustrate the phase-velocity-ordering of modes, with rescatter and LDI of rescatter intermediate between SRFS and SRBS.

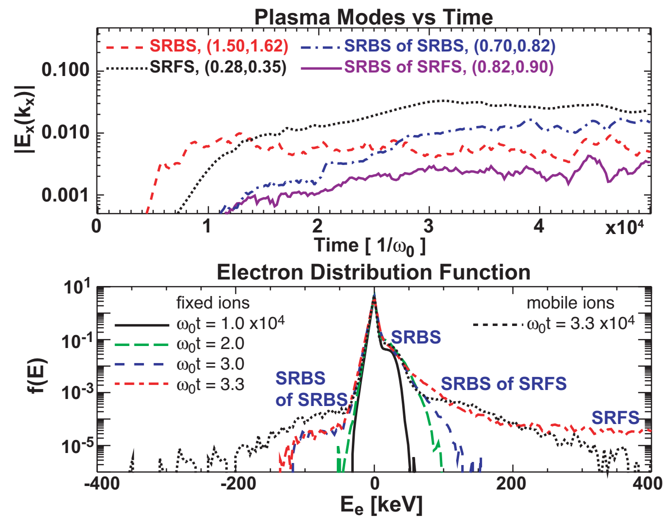

FIG. 3: Top) Temporal evolution of the SRS EPW wavenumbers for $k_x c/\omega_0$ within the labeled bounds; fixed ion simulation. Bottom) Electron energy spectrum; heating due to LDI not labelled.

[8]. Since v_{max} and $\mathcal{E}_{max}$ above depend on $\Delta\Phi$, we consider the wavebreaking derivation of [9] which shows that extrema in $\Phi(\overline{v})$,

$$\Phi(\overline{v}) = -\overline{v} + \frac{\overline{v}^2}{2} + \frac{\overline{\beta}}{2(1-\overline{v})^2} + c_0, \tag{1}$$

occur for roots of $\overline{E}(\overline{v})$, where,

$$(\overline{E}(\overline{v}))^2 = \overline{E}^2_{peak} - \overline{v}^2 + \overline{\beta}\left[\frac{2}{3(1-\overline{v})^3} - \frac{1}{(1-\overline{v})^2} + \frac{1}{3}\right].$$

Here a waterbag distribution is assumed, $\overline{E} = eE/m\omega_p v_\phi$ is the normalized electric field, $\overline{v} = v/v_\phi$, $\overline{\beta} = 3(v_{th}/v_\phi)^2 = 3k^2\lambda_D^2/(1+3k^2\lambda_D^2)$, and c_0 is an arbitrary constant. Assuming $\overline{E}_{peak}$ is the wavebreaking amplitude, two of the roots correspond to fluid velocities at the extrema in Φ at wavebreaking. We can substitute these two roots into Eqn. 1 to calculate $\Delta\Phi$ between the extrema and substitute $\Delta\Phi$ into the above expressions for v_{max} and $\mathcal{E}_{max}$ [10]. Figure 2 top-left shows v_{max}/v_ϕ as a function of β, from which it is seen that for $\beta > 0.1$ ($k\lambda_D \gtrsim 0.18$) the difference between v_{max} and v_ϕ is no bigger than v_ϕ, i.e., $v_{max} < 2v_\phi$. Figure 2 top-right shows $\mathcal{E}_{max}$ assuming that $T_e = 2.5$ keV, where the dotted line uses $\mathcal{E}_{max} = \frac{1}{2}mv^2_{max}$ and the solid line includes relativistic corrections. In simulations, we find that E_{peak} (Φ_{peak}) for the SRBS wave is typically $\lesssim 2/3$ of the wavebreaking estimate, so these curves should be viewed as a limit.

The appropriate v_ϕ and $\mathcal{E}_\phi$ (kinetic energy for a particle at v_ϕ) for the various EPWs are shown in Figure 2-bottom. The plots in combination show that SRBS does not longitudinally accelerate electrons to 100 keV kinetic energies. Trapped particles with additional transverse velocity components may reach such energies, as may have occurred in L. Yin *et al.* [11], but we leave this for future work. For rescatter, on the other hand, with higher v_ϕ (and lower β), 100 keV is well within range. Rescatter EPWs, as well as their LDI decay EPWs, are potential producers of 100 keV electrons.

In this article, we present one and two dimensional (1D and 2D) simulations using the electromagnetic PIC code OSIRIS [12]. The first simulation is 1D with $T_e = 2.5$ keV, electron density $n_e/n_{cr} = 0.09$ ($k\lambda_D \approx 0.35$ for SRBS), and both fixed and mobile ions with $ZT_e/T_i = 3$ and $M_i/m_e = 1836$. The laser wavelength $\lambda_0 = 0.351\mu$m and intensity $I_0 = 3 \times 10^{15}$ W/cm^2. 16384 cells were used with 512 particles per cell with quadratic particle shapes to simulate a plasma of length 180 μm corresponding to an $f/8$ speckle of length $8f^2\lambda_0 = 180\mu$m. The second simulation is exactly similar (with mobile ions) with the exception that it has a linear density gradient from $n_e/n_{cr} = 0.09$ to 0.10 over the domain length. Finally, the third simulation is 2D with $T_e = 3$ keV, $n_e/n_{cr} = 0.10$, $ZT_e/T_i = 2$, domain size 200 x 15 μm^2, 16384 x 512 cells, 256 particles per cell, and the laser is focused from $I_0 = 3\times 10^{15}$ W/cm^2 at the simulation edge to $I_0 = 5 \times 10^{15}$ W/cm^2 at focus with a focal spot size of 2.6 μm ($8\lambda_0$). All simulations have absorbing boundaries for the fields in all directions and have the plasma extending up to the boundary in all directions; exiting particles are re-injected with a random velocity from the initial background Maxwellian distribution. The laser propagates along $\hat{x}$, is polarized in $\hat{z}$ (perpendicular to the 2D plane), and has a constant amplitude after a rise time $\omega_0 t_{rise} = 300$.

First we consider the 1D run with immobile ions and homogenous density $n_e/n_{cr} = 0.10$. The temporal evolution of the SRS EPW wavenumbers can be seen in Figure

3, along with the corresponding temporal evolution of the electron distribution function. SRBS grows first, as it has the largest growth rate. SRFS follows, and soon afterwards the scattered light from both SRFS and SRBS has grown to sufficient amplitude that rescatter grows.

The hot electron tails in the distribution follow a different progression. The forward-traveling EPW phase momenta ($p_e/m_e c = \gamma v_\phi$) increase from SRBS (0.26) to SRBS of SRFS (0.56) to SRFS (2.4), with electrons at those speeds having kinetic energies of 17, 75, and 820 keV respectively. Electron trapping by SRBS starts at $\omega_0 t \approx 10000$; this process does not accelerate electrons above 70 keV. SRFS grows to a mode amplitude larger than SRBS by $\omega_0 t = 20000$, but normalized to its wavebreaking value it is smaller so it does not trap particles and has no immediate effect on the hot electron tail. Electrons begin to be accelerated to energies above 70 keV by the rescatter that develops at $\omega_0 t \approx 20000$, and by $\omega_0 t \approx 33000$ electrons have been accelerated to sufficient energies by the rescatter that SRFS can trap electrons, accelerating them beyond 250 keV all the way up to 1 MeV.

Though not shown, the maximum EPW amplitude in the region of SRFS activity is $eE/mv_\phi\omega_p \approx e\Phi/mv_\phi^2 \approx 0.37$ at $\omega_0 t \approx 33000$. Using $v_\phi = 0.93c$, the energy an electron needs in order to be trapped is 140 keV ($v = 0.62c$). Since SRBS only generates electrons with energies less than approximately 70 keV, this illustrates why SRFS requires the intermediate step of rescatter. This is consistent with Figure 3 where the hot tail sweeps to higher energies once rescatter heats electrons to 140 keV. With heating by both rescatter and SRFS, approximately 0.1% of the electrons get heated above 100 keV.

Figure 3-bottom also shows electron heating due to SRBS of SRBS in the negative direction with energies of order 100 keV. This tail requires longer to develop, as there is only one EPW in that direction and the rescatter must therefore be driven to sufficient amplitude.

The number of both forward and backward propagating EPWs is larger if we allow ions to be mobile. Figure 3-bottom shows a representative distribution from an equivalent simulation with mobile ions illustrating roughly similar electron heating, but the physics behind it is more complex due to LDI and the resulting counter-propagating EPWs that can be generated for each decaying EPW.

While we do not see Brillouin scattering for our parameters, we do see LDI. LDI can potentially saturate SRS, but each SRS process (SRBS, SRFS, and rescatter) has a different value of $k\lambda_D$ and is in a different kinetic regime. Both rescatter processes are SRBS processes and scale like SRBS, although the SRBS and SRFS scattered light waves have longer wavelengths and lower frequencies than the incident laser, resulting in comparatively lower SRBS intensity thresholds, higher growth rates, and rescattered EPWs less affected by kinetic effects and

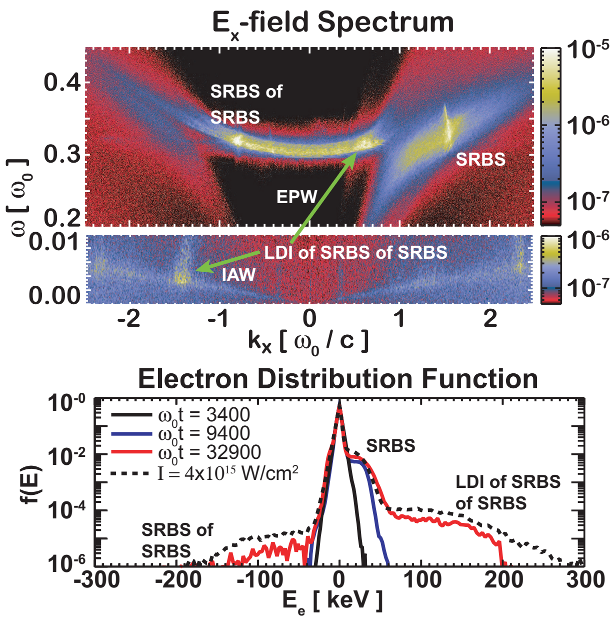

FIG. 4: Top) Frequency vs wavenumber of E_x-field. Bottom) Electron distribution versus electron kinetic energy for $I_0 = 3$ (solid) and 4 (dashed) $\times 10^{15}$ W/cm^2, where +/- represent forward/backward traveling electrons.

more affected by LDI. We have performed other simulations varying laser intensity, density, and temperature, and we have seen similar heating by rescatter provided the scattered light is intense enough. However, even for strong SRS, rescatter can not grow at densities above its quarter-critical density, which for scattered light of frequency $\omega \approx \omega_0 - \omega_p$ is $n/n_{cr} \approx 0.11$. On the other hand, for lower densities such as $n/n_{cr} < 0.09$, the growth rates of all SRS processes decrease, likewise making rescatter less likely; density gradients will also act to quench SRS instabilities.

We turn now to our second simulation set-up, a scenario in which SRFS is quenched by the density gradient; density rises linearly from $n_e/n_{cr} = 0.09$ to 0.10 over the domain length. Only one variety of rescatter is present (SRBS of SRBS). In this case, the impact of LDI is therefore simplified.

The spectrum of plasma modes can be seen in Figure 4-top. Figure 4-bottom shows that rescatter (here SRBS of SRBS) again accelerates electrons up to energies of 100-200 keV. The EPW from LDI decay of rescatter also heats electrons, and as it travels in the opposite direction as the rescatter EPW, the combined instabilities generate energetic electrons in both directions. One reason that the electrons going forward reach higher energies than those going backward is because the LDI decay EPW has a slightly lower wavenumber compared to the rescatter EPW and therefore a slightly higher phase velocity. The hot tail due to LDI therefore extends to higher energies than the tail due to rescatter. Furthermore, even though

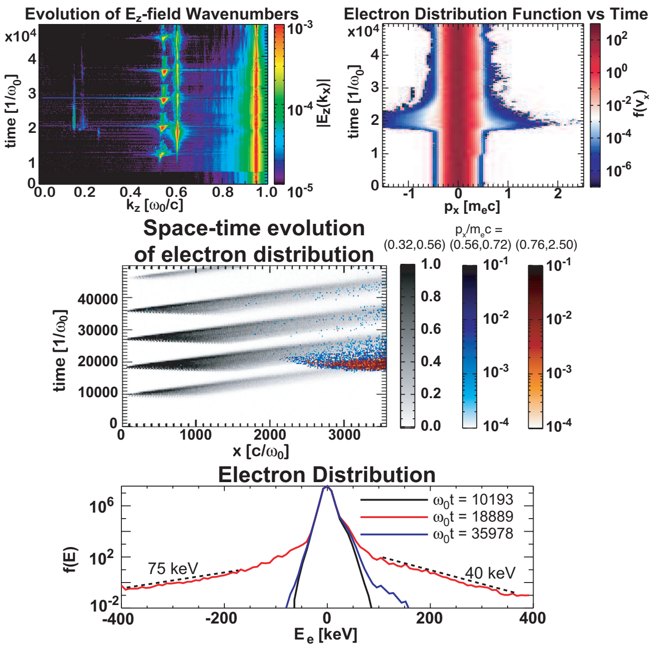

FIG. 5: Top) Temporal evolution of transverse E-field wavenumbers along the simulation center (top-left) and longitudinal electron distribution spatially averaged over x and y (top-right). Middle) Charge density of electrons at v_ϕ of BSRS (grey), SRBS of SRFS (blue), and SRFS (orange). Bottom) Energy distribution; includes transverse momentum with ± referring to the sign of p_x.

the LDI EPW interacts with the electron distribution at higher velocities, it heats more total electrons than the rescatter EPW since it also interacts with the previously formed hot tail from the original SRBS.

If we apply our earlier theoretical estimate of electron v_{max} to the rescatter and LDI EPWs, we can test it against the electron spectrum shown Figure 4. The EPWs have $v_\phi \approx 5.6 v_{th}$ for rescatter of SRBS and $6.4 v_{th}$ for LDI of rescatter. The electron kinetic energies corresponding to the theoretical limit (Fig. 2) of v_{max} are $\approx$ 200 keV for SRBS and 300 keV for LDI. These indeed bound the upper edges of the flat tails in the plotted distribution in Figure 4, even for an exactly similar case with higher laser intensity. The low-velocity end of the hot tails correspond approximately to $\mathcal{E}_\phi \approx mc^2(\gamma_\phi - 1)$ ($\approx$ 44 and 61 keV).

Finally, we present results from a 2D simulation of a single speckle in a uniform plasma. Figure 5-top-left shows the temporal evolution of wavenumbers for the E_z (transverse) field along the central axis. The bursty mode at $kc/\omega_0 \approx 0.5$ corresponds to SRBS, while the steadily growing mode at $kc/\omega_0 \approx 0.6$ that peaks at $\omega_0 t \approx 17000$ corresponds to SRFS (the anti-Stokes mode is also present at $kc/\omega_0 \approx 1.3$). Rescatter of both light waves is present, with SRBS of SRBS at $kc/\omega_0 \approx 0.20$ and SRBS of SRFS at $kc/\omega_0 \approx 0.15$ starting at $\omega_0 t \approx$ 17000. Corresponding rescatter plasma wave modes are seen in the E_x field (not shown), as well as broadband signals from modes that grow after $\omega_0 t \approx 17000$ due to LDI. SRBS EPWs may be affected by 2D kinetic effects such as transverse localization, wave-bowing, and filamentation [13–16], though the rescatter EPWs have $k\lambda_D \approx 0.2$ and are more affected by LDI. Studying in detail the interplay of these effects when such a wide variety of EPWs are present, each in a different kinetic regime, is left for future work.

The electron distribution shown in Figure 5-top-right flattens slightly at $\omega_0 t = 10000$ due to the first burst of SRBS, followed by much more energetic tails at $\omega_0 t =$ 18000 due to rescatter and LDI of rescatter. Though not shown here, the electron phasespace reveals that the positive momentum tail is caused by SRBS of SRFS and the negative momentum tail by LDI of SRBS of SRFS. The importance of trapped electron bootstrapping between SRBS and rescatter can be seen in the middle plot of Figure 5, where the charge density amplitude in electron phasespace, summed over the transverse direction, is plotted as a function of space and time for three different ranges of electron momenta. The phasespace bins $p_e/m_e c = (0.32, 0.56)$, $(0.56, 0.72)$, and $(0.76, 2.50)$ cover v_ϕ of the EPWs due to SRBS, SRBS of SRFS, and SRFS respectively. With SRBS (SRFS) growing behind (in front of) the laser focus ($x\omega_0/c = 1790$), electrons heated by SRBS first have to cross the simulation length before interacting with the region where SRFS (and rescatter of SRFS) has grown. After they cross (as shown in grey), the rescatter can interact with these electrons and accelerate them further. Blue shows electrons heated by rescatter, which is seen to occur when electrons heated by SRBS enter the region of rescatter, while orange shows further acceleration by SRFS. LDI limits SRFS for $\omega_0 t > 20000$, and thereby also rescatter of SRFS. At $\omega_0 t \approx 18000$, those hot electrons with kinetic energies above 100 keV have a forward-going kinetic energy flux of approximately 3% of the total incident laser poynting flux, while subsequent fluxes at $\omega_0 t \approx 36000$ and 43000 are both $\approx 0.2\%$.

The electron distribution in energy is shown in Figure 5-bottom, where one can see that electrons are not accelerated to 100+ keV energies until rescatter has grown ($\omega_0 t > 17000$). Fitted lines for temperatures show that the range of electron energies, not the slope of the distribution, identifies which plasma wave (instability) is responsible for those hot electrons, a conclusion which could also be drawn from Figures 3 and 4.

The range of energies shown in this article is consistent with reported hot electron measurements from NIF and shows that SRS rescatter should be considered as a source of 100 keV electrons. While the results here are limited to single speckles with intensities at the higher end of expected hot spot intensities (e.g. including cross-beam energy transfer and overlapping inner beams [17, 18]), one might reasonably assume that scattered light will be amplified to levels seen here as it travels through multiple speckles. Multi-stage electron acceleration between EPWs has been shown in two-plasmon decay simulations [19] and may generate 100 keV electrons in multi-speckle SRS; we believe this topic is worth further study.

This work was supported by DOE under Grant No. DE-FG52-09NA29552 and by NSF under Grant No. NSF-Phy-0904039. Simulations were carried out on the UCLA Hoffman2 cluster and NERSC's Franklin and Hopper systems.

[1] E. L. Dewald *et al.*, Rev. Sci. Inst. **81**, 10D938 (2010).
[2] P. Michel *et al.*, Phys. Rev. E **83**, 046409 (2011).
[3] D. E. Hinkel *et al.*, Phys. Plasmas **11**, 1128 (2004).
[4] K. Estabrook, W. L. Kruer, and B. F. Lasinski, Phys. Rev. Lett. **45**, 1399 (1980); K. Estabrook and W. L Kruer, Phys. Fluids **26**,1892 (1983).
[5] W. B. Mori, M.S. thesis, University of California, Los Angeles, 1984.
[6] P. Bertrand *et al.*, Phys. Plasmas **2**, 3115 (1995).
[7] A. B. Langdon and D. E. Hinkel, Phys. Rev. Lett. **89**, 015003 (2002).
[8] T. P. Coffey, Phys. Fluids **14**, 1402 (1971).
[9] W. B. Mori and T. Katsouleas, Phys. Scr. **T30**, 127 (1990).
[10] More detail will be provided in a longer paper.
[11] L. Yin *et al.*, Phys. Plasmas **19**, 056304 (2012).
[12] R. G. Hemker. Ph.D. thesis, University of California, Los Angeles, 2000; R.A. Fonseca *et al.*, Lecture Notes in Computer Science **2331**, 342 (2002); R.A. Fonseca *et al.*, Plasma Physics and Controlled Fusion **50**, 124034 (2008).
[13] J. E. Fahlen, B. J. Winjum, T. Grismayer, W. B. Mori, Phys. Rev. E **83**, 045401(R) (2011).
[14] J. Banks *et al.*, Phys. Plasmas **18**, 052102 (2011).
[15] L. Yin *et al.*, Phys. Plasmas **15**, 013109 (2008).
[16] H. A. Rose and L. Yin, Phys. Plasmas **15**, 042311 (2008).
[17] P. Michel *et al.*, Phys. Plasmas **17**, 056305 (2010).
[18] D. E. Hinkel *et al.*, Phys. Plasmas **18**, 056312 (2011).
[19] R. Yan *et al.*, Phys. Rev. Lett. **108**, 175002 (2012).